ACS APPLIED MATERIALS & INTERFACES

Research Article

www.acsami.org

Spatially Controlled Surface Energy Traps on Superhydrophobic Surfaces

Athanasios Milionis,*[,†,⊥] Despina Fragouli,[†] Luigi Martiradonna,[‡] George C. Anyfantis,[†] P. Davide Cozzoli,[§,∥] Ilker S. Bayer,[†] and Athanassia Athanassiou*[,†]

[†]Nanophysics, Istituto Italiano di Tecnologia (IIT), Via Morego 30, 16163 Genova, Italy

[‡]Center for Biomolecular Nanotechnologies (CBN) at UNILE, Istituto Italiano di Tecnologia (IIT), Via Barsanti, 73010 Arnesano, Lecce, Italy

[§]Dipartimento di Matematica e Fisica "E. De Giorgi", Universita del Salento, via per Arnesano, 73100 Lecce, Italy

[∥]National Nanotechnology Laboratory (NNL), CNR Istituto Nanoscienze, c/o Distretto Tecnologico, via per Arnesano km 5, 73100 Lecce, Italy

Supporting Information

ABSTRACT: Water wetting and adhesion control on polymeric patterns are achieved by tuning the configuration of their surface's structural characteristics from single to dual and triple length-scale. In particular, surfaces with combined micro-, submicrometer-,and nanoroughness are developed, using photolithographically structured SU-8 micro-pillars as substrates for the consecutive spray deposition of polytetrafluoroethylene (PTFE) submicrometer particles and hydrophobically capped iron oxide colloidal nanoparticles. The PTFE particles alone or in combination with the nanoparticles render the SU-8 micropillars superhydrophobic. The water adhesion behaviour of the sprayed pillars is more complex since they can be tuned gradually from totally adhesive to completely non adhesive. The influence of the hierarchical geometrical features of the functionalized surfaces on this behaviour is discussed within the frame of the theory. Specially designed surfaces using the described technique are presented for selective drop deposition and evaporation. This simple method for liquid adhesion control on superhydrophobic surfaces can find various applications in the field of microfluidics, sensors, biotechnology, antifouling materials, etc.

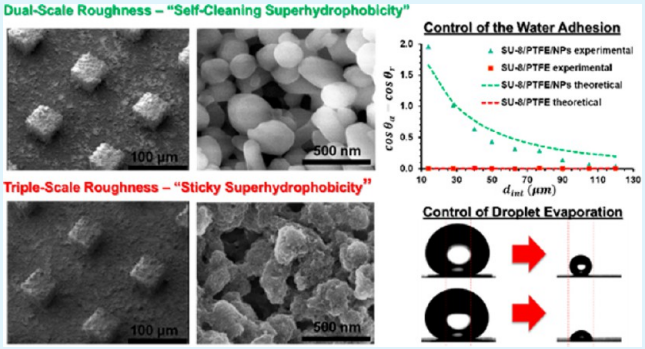

KEYWORDS: *water adhesion, surface roughness, superhydrophobicity, polymeric micropillars, spray-coating*

1. INTRODUCTION

Self-cleaning superhydrophobic surfaces with apparent water contact angle (APCA) above 150° and very low contact angle hysteresis (CAH) have attracted the attention of many studies during the past few years because of their importance in fundamental research but also in practical applications.[1−8] More recently, emerging research is focused on a different type of surfaces, which are superhydrophobic in terms of APCA but simultaneously exhibit high adhesion,[9−11] aiming for the fabrication of coatings performing intelligent functions, such as directional drop movement, drop transportation, storage of binary data, etc.[12−15] In fact, the possibility to control spatially the water adhesion on superhydrophobic surfaces without altering the APCA is a promising aspect for the development of smart devices where multiple functions are performed on their entire surface.[15] Many of the surfaces proposed up to now have intrinsic limitations prohibiting their use in specific applications. Most of them do not exhibit spatially controlled, but rather a uniform adhesion throughout their surface, excluding their use in applications like targeted delivery of biomolecules or localized chemical reactions.[16−19] Moreover, in certain occasions where external stimuli are needed for the control of adhesion, the incorporation of additional components in an integrated system should be considered.[14,15,20−22] In other cases, although spatial control of adhesion is achieved, in the highly adhesive areas the APCA is significantly lower than 150° so the droplets may lose their spherical shape.[23]

One strategy to render solid substrates superhydrophobic with controlled adhesion is the deposition of different types of particles on flat or rough substrates to obtain multiscale roughness. Such approaches may include the use of different shaped micro-, submicro-, and nanomaterials composed by PTFE,[24] metal oxides,[16,24,25] silica,[26] lycopodium,[27] etc. Following a similar approach, in a previous study we deposited the right combinations of submicrometer and nanoparticle dispersions on a micropatterned surface in order to create a

Received: October 16, 2013
Accepted: December 26, 2013
Published: December 26, 2013

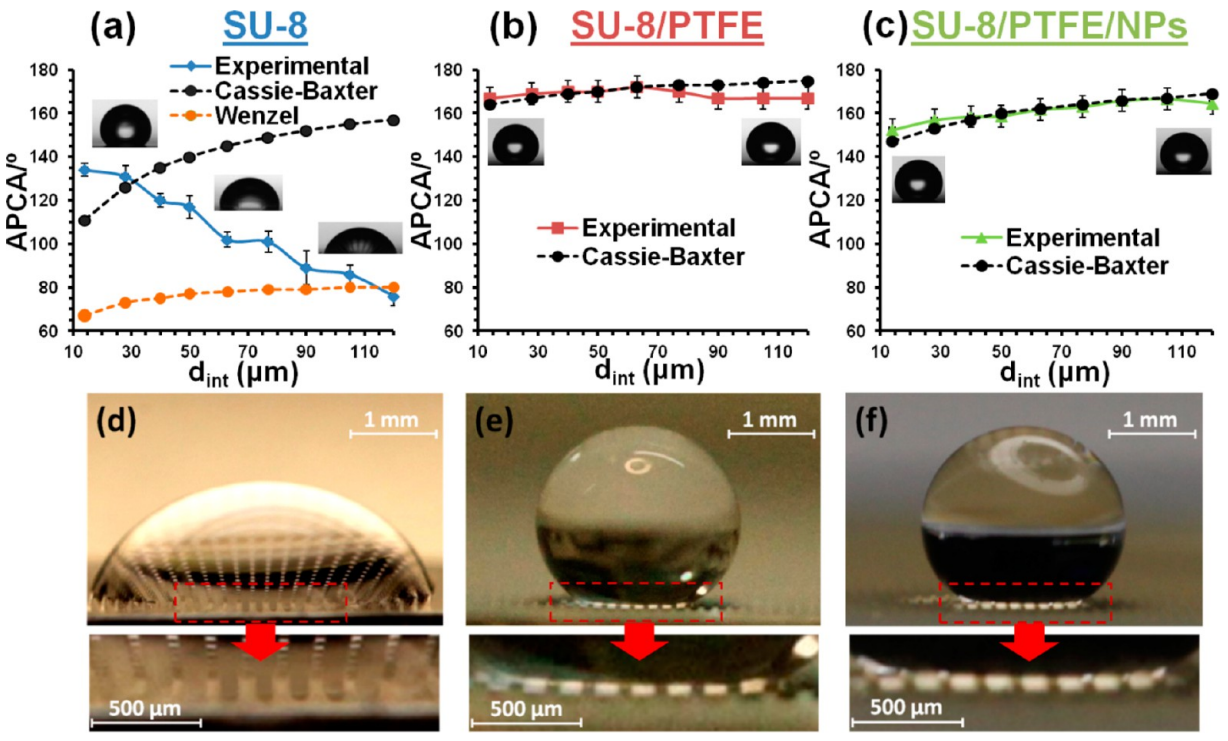

Figure 1. Dependence of the experimental and theoretical contact angles on the interpillar distance of (a) SU-8, (b) SU-8/PTFE, and (c) SU-8/PTFE/NPs patterns. Images of drops placed on (d) SU-8, (e) SU-8/PTFE, and (f) SU-8/PTFE/NPs patterns, with interpillar distance 120 μm. Corresponding insets: Higher magnification in the part of the substrate in contact with the drop.

superhydrophobic substrate that turns from self-cleaning to highly adhesive.[24] In that paper only the two extreme adhesion states were achieved, namely the "lotus effect" and the "petal effect" with no gradual tuning between them.

In the present paper, we advanced our research in the field demonstrating that control of the micro-roughness results in total control and tuning of the CAH of the developed superhydrophobic surfaces. In fact, the latter demonstrate gradual tuning of the CAH ranging from extremely low to extremely high values with different intermediate states, depending on the induced underlying multiscale roughness. We also developed a theoretical model that can predict these CAH values by taking in consideration the different geometry and chemistry that characterizes each roughness scale used in the experiments. Finally, we demonstrate for the first time how this technique can be utilized for the spatial control of water adhesion, through applications regarding spatial manipulation of water droplets and controlled evaporation on superhydrophobic spots. In particular, since highly adhesive areas on the surfaces can be purposely fabricated using shadow masks, such predesigned spots can successfully entrap spherical water droplets without any use of external stimuli, rendering the substrates good candidates for targeted deposition of water-soluble substances on predefined surface locations. The produced substrates can also be incorporated in other applications as sophisticated systems regarding liquid transportation, detection of biomaterials at ultralow concentrations, biochemical separation, and localized chemical reactions.[28−30]

2. EXPERIMENTAL SECTION

Materials. SU-8 3050 photoresist (Microchem, U.S.A.) was used as received. Polytetrafluoroethylene (PTFE) sub-micrometer spherical particles (diameter 200−300 nm) in powder form and all solvents used were purchased from Sigma Aldrich. Colloidal iron oxide nanoparticles (NPs) were synthesized by a wet-chemical synthetic approach as described in ref 24.

Preparation of the Spray-Coated SU-8 Micropillars. SU-8 films were prepared by spin-coating as previously described.[24] Sodalime masks of square shaped patterns (42 μm side) from Deltamask Netherlands, with various inter-square distances were used for the exposure of the spin-coated samples. Square micropillars of 33 μm height, 42 μm side and inter-pillar distances (d_{int}) varying from 14 μm up to 120 μm were obtained. Subsequently, the samples were spray-coated with a PTFE/acetone dispersion (3 wt %) and a NPs/chloroform dispersion (0.06 wt %) following the same method as in ref 24. For the localized spray-coating of the NPs a circular mask with a conical shape was used in order to guide the flow of the NPs in a confined hole of 0.5 mm diameter. After spraying the NPs solution through this mask, circular sprayed patterns of approximately 0.85 mm diameter were obtained.

Characterization of the Samples. Measurements of the Apparent Water Contact Angle (APCA), as defined by Marmur,[31] were carried out using a KSVCAM200 contact angle goniometer, Kruss, Germany. Multiple measurements were taken by gently depositing 10 μL drops of deionized water on several samples prepared with the same procedure. The area of the drop in contact with the surface was sufficient enough to experience the periodicity of the pattern. To calculate the CAH, the advancing and receding angles were measured by dispensing and retracting water until a motion of the contact line on the surface was observed.[31] The CAH is defined as the difference between the advancing and receding angle, thus giving a measurement of the water adhesion to the patterned surfaces. For the surface topography analysis, scanning electron micrographs were collected with a Nova NanoSEM200 manufactured by FEI. Finally, the optical images were acquired with a Canon EOS 5D Mark II camera equipped with a Canon EF 100 mm f/2.8 L IS USM Macro objective lens.

3. RESULTS AND DISCUSSION

The initial modification induced to the pillared patterns in order to tailor their wetting properties, is related to their

geometry. Indeed, the increase of the pillars' distance d_{int} results in the gradual conversion of these substrates from hydrophobic to hydrophilic (Figure 1a). However, the spray deposition of hydrophobic PTFE[6] spherical submicrometer particles onto the micro-pillars turns the surfaces to superhydrophobic with APCAs higher than 165° in all cases, while the corresponding flat surface shows $APCA_{flat.SU-8/PTFE}$ 159 ± 8° (Figure 1b). When spherical iron oxide colloidal NPs with hydrophobic surfactants are subsequently sprayed onto the PTFE coating,[24] the APCAs remain above 150° (superhydrophobic) in all cases, slightly increasing with the d_{int} until they reach almost 160°, for pillars separated by 120 μm (Figure 1c). The corresponding flat SU-8/PTFE/NPs substrates show $APCA_{flat.SU-8/PTFE/NPs}$ of 135 ± 10°.

The wetting behaviour of surfaces with a homogeneous roughness is generally predicted by the Cassie-Baxter's[32] and the Wenzel's models.[33] The application of such models to the square-type pillar-geometries[34] used in this study, reveals the way the water drops are assembled on the fabricated surfaces. The Cassie–Baxter model assumes that air gets trapped into the recessed regions of a rough surface when a water droplet is placed on it. In this way the water droplet wets only partially the surface. The model describes the APCA of the rough surface as follows:

$$\cos(\theta_{CB}) = f_{SL}[\cos(\theta_Y) + 1] - 1 \quad (1)$$

where θ_{CB} is the APCA of the rough surface, f_{SL} is the fraction of the solid surface in contact with the liquid, and θ_Y is the Young's angle, that is, the contact angle of the liquid on the corresponding flat surface with the same chemical characteristics. In our case, f_{SL} is calculated using the following equation:[34]

$$f_{SL} = \frac{1}{\left(\frac{d_{int}}{a} + 1\right)^2} \quad (2)$$

where α is the width of the pillars (42 μm).

According to the Wenzel's model, the water seeps within the recessed regions of the surface, tending to increase the interfacial contact area shared with the solid until a complete wetting condition is eventually achieved. The wettability behaviour of a rough surface is then described by the following equation:

$$\cos(\theta_W) = R_f \cos(\theta_Y) \quad (3)$$

where θ_W is the APCA on the rough surface and R_f is the roughness factor, defined as

$$R_f = \frac{A_{SL}}{A_F} \quad (4)$$

where A_{SL} is the solid–liquid contact area and A_F is the projection of the solid–liquid contact area on the horizontal plane.

For the pillar geometries used in this work the roughness is defined as[34]

$$R_f = 1 + \frac{4f_{SL}}{(a/H)} \quad (5)$$

where H is the height of the pillars (33 μm) and f_{SL} is given by eq 2.

For the pristine SU-8 micro-pillars, Figure 1a shows that both Cassie–Baxter's and Wenzel's model predict that the APCAs increase with increasing d_{int}, in contrast with the experimental evidence. This indicates that for increasing d_{int}, a transition from Cassie to Wenzel state occurs with the water drops totally wetting the most distant pillars (Figure 1d), as already shown elsewhere.[35,36] In the cases of SU-8/PTFE or SU-8/PTFE/NPs samples, the predicted Cassie-Baxter values are very close to the experimental ones (Figure 1b, c), while the values predicted by the Wenzel model are not coherent with the measured APCAs (data not shown). In fact, as shown in the images of Figure 1e and 1f, air stays trapped under the water drops even on the samples with the largest d_{int}, allowing us to conclude that the spray-coated patterns exhibit Cassie-type superhydrophobicity.

The effect of the nanoroughness in the APCA values between the SU-8/PTFE and SU-8/PTFE/NPs is minimal but on the other hand is essential for controlling the CAH of the substrates. Regarding the topography, the SU-8 patterns are very smooth and uniform in the micro- and nanoscale as confirmed by the high-magnification SEM image in Figure 2a2.

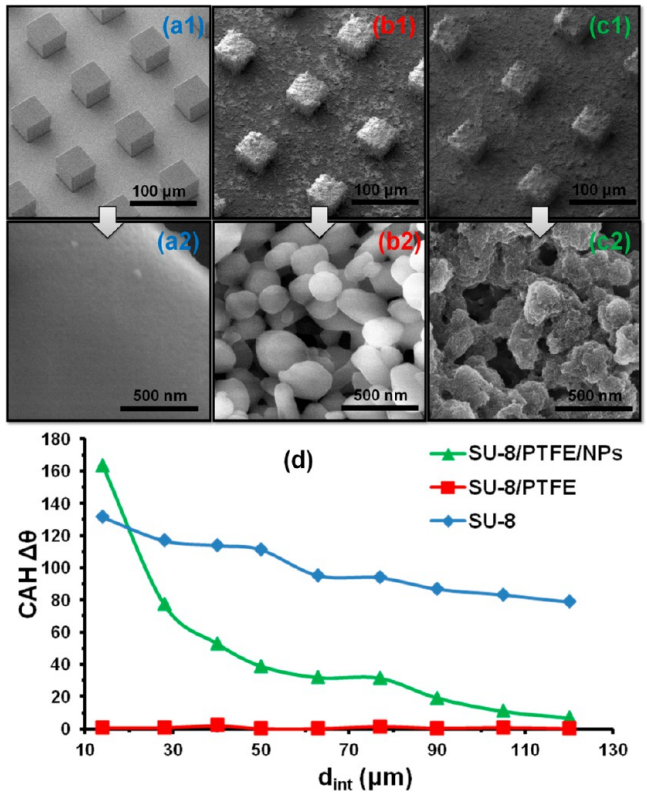

Figure 2. Low-magnification tilted-view SEM images of (a1) SU-8, (b1) SU-8/PTFE, and (c1) SU-8/PTFE/NPs micro-pillars, and their corresponding high-magnification top-view images (a2), (b2), and (c2). (d) CAH values for the SU-8, SU-8/PTFE and SU-8/PTFE/NPs substrates for different d_{int}.

However, when the PTFE particles are sprayed on the pillars, the latter retain their microscale geometry adding submicrometer roughness on their surfaces, as shown in Figure 2b1,2 where the submicrometer particles are clearly identified, and the pillars are well distinguished. Subsequent spray deposition of hydrophobic iron oxide NPs on the PTFE coated micro-pillars results in pillar structures with hierarchical submicrometer- and nanoroughness. Indeed, Figure 2c2 shows that the underlying PTFE particles are fully covered by the NPs,

without leaving uncoated voids, providing the additional nanorough characteristics.

These successive roughness modifications have an interesting impact in the CAH. Up to now, the CAH on regular pillar-like hydrophobic surfaces has been investigated concluding that in a Wenzel state the CAH is proportional to the surface micro-roughness induced by the pillars, which changes with the d_{int}.[37] On the contrary, in a Cassie−Baxter state, the pillar-micro-roughness does not contribute to the CAH. In a Cassie−Baxter state, the CAH depends exclusively on the solid-liquid fraction f_{SL}. Other studies examine the pinning effects on the three-phase contact line in the edges of the pillars and their influence in the depinning force or the sliding angle of water droplets, concluding that for increased pillar density these parameters follow the same positive correlation (sliding angle and depinning force increase).[38−40] So, up to now, the influence of the CAH has been theoretically examined only on surfaces that exhibit one-scale roughness. The special case where such patterned surfaces exhibit multiple scale roughness has been examined only very recently, but for substrates with the same chemistry throughout their entire topography.[41] Combinations of different wetting states due to multiple scale rough substrates with each roughness scale to present diverse chemical characteristics, like in the present study, to the best of our knowledge, have not been presented so far.

Herein, as shown in Figure 2d the water adhesion on the pristine SU-8 pillars is extremely high, being always higher than 79° as expressed by the difference ($\Delta\theta$) between the advancing and receding angles (CAH for flat SU-8 = 20°). However, after covering the SU-8 pillars with a PTFE particles layer by spray-coating, a dramatic decrease of the CAH for all d_{int} is observed. Indeed, the CAH remains always below the value of 2° (CAH for flat SU-8/PTFE = 4°). When the subsequent layer of hydrophobic iron oxide NPs is sprayed on top of the PTFE layer, the resulting SU-8/PTFE/NPs surfaces demonstrate a tunable CAH, which decreases as the pillars become more distant. At small-pillar spacing, $d_{int} \leq 35$ μm, the receding contact angles are significantly lower compared to the advancing ones, resulting in CAH > 70°. It should be mentioned that the CAH of the pattern with $d_{int} = 14$ μm is higher than the respective CAH for the corresponding flat surface (CAH for flat SU-8/PTFE/NPs = 131°), since the depinning forces for closely packed pillars are greater than those acting on a planar surface, as also reported recently by Xu et al.[38] The high adhesion of these multilayer pillars is also demonstrated by the fact that the drops stay adhered on their surface even for 180° tilt angles. At $d_{int} > 35$ μm, the CAH gradually decreases, reaching CAH < 10° for $d_{int} > 85$ μm and tilt angles down to 23° for the maximum d_{int} used (120 μm). Such variations can be exclusively attributed to the changes in the distance between the underlying micropillars since this is the only variable parameter. Specifically, this tunable micro-roughness in combination with the induced submicrometer and nanoroughness affects the surface adhesion significantly (Figure 2).

The general increase in the CAH values of the SU-8/PTFE/NPs system compared to the SU-8/PTFE can be attributed mainly to the pinning effects at the water/NPs interface throughout and at the edges of the pillars.[41,42] Such pinning effects are observed even if air pockets remain trapped under the droplet in the inter-pillar spacing, as demonstrated in Figure 1c and f. Actually, the water drops on the SU-8/PTFE/NPs samples may stay on the top of the pillars with air pockets trapped in the inter-pillar areas, even though locally the water can penetrate because of local capillary effects in the nano-rough features created by the NPs exhibiting a Wenzel-type wetting on the top of the pillars. These pinning effects on the nano-features of the surface do not affect the APCA, leading however to an increase in the CAH.

Summarizing, in the micro-scale the wetting is of Cassie-type as demonstrated in Figure 1 for all the sprayed patterns (SU-8/PTFE and SU-8/PTFE/NPs). However, in the nano-scale induced by the sprayed hydrophobic iron oxide NPs, there is an evidence of pinning phenomena occurring that increase the CAH (Figure 2d). This increase of the CAH is expected to be enhanced when the NPs/water interface becomes larger, thus for narrower inter-pillar spacing, as demonstrated in Figure 2d.

To confirm these findings, our results were compared with existing theoretical models that calculate the CAH on patterned superhydrophobic surfaces. Specifically, Bhushan et al.[42] have shown that the CAH of water drops that reside on the top of micropillar-patterned structures, thus described by the Cassie−Baxter wetting behaviour, can be predicted by the following equation:

$$\cos\theta_\alpha - \cos\theta_r = R_{fsub} f_{SL}(\cos\theta_{\alpha 0} - \cos\theta_{r0}) + H_r \quad (6)$$

where θ_α and θ_r are the advancing and receding APCAs for the patterned surface, respectively, and $\theta_{\alpha 0}$ and θ_{r0} are the advancing and receding angle for a smooth surface of the same chemistry as the rough one. f_{SL} is the solid fraction of the entire micropatterned structure in contact with the liquid, and can attain values smaller than 1. R_{fsub} is the roughness factor on a single pillar's surface. In our case the top of the pillars show submicrometer and nano-rough characteristics induced by the sprayed particles. For reasons of simplicity, from now on, all the types of roughness below 1 μm will be mentioned as submicrometer roughness. H_r is the term that accounts for the hysteresis because of the slip-stick movement of the drop on the edges of the pillars. This term is proportional to the density of the pillars

$$H_r = c S_f^{\,2} \quad (7)$$

where c is a non-dimensional proportionality constant and S_f is the spacing factor, which in the present case (square shaped micropillars) is

$$S_f = \frac{a}{(a + d_{int})} \quad (8)$$

Equation 6 considers that the submicrometer rough features on the top of the pillars are wetted by the water drops showing locally a Wenzel-type wetting behaviour. In this case R_{fsub} is given by the ratio of the submicrometer-rough wetted area to its projection, and takes values greater than 1. We combine the eqs 6−8 and 2 to obtain the following equations that describe the CAH for a superhydrophobic micropillar-patterned surface, with overall Cassie−Baxter-type wetting behaviour, but locally, on the top of the pillars, Wenzel-type wetting behaviour

$$\cos\theta_\alpha - \cos\theta_r = A_W f_{SL} \quad (9)$$

where A_W is a positive non-dimensional constant that equals

$$A_W = R_{fsub}(\cos\theta_{\alpha 0} - \cos\theta_{r0}) + c \quad (10)$$

On the other hand when the water drops do not penetrate into the areas between the micropillars, there is another possibility that they reside also on the top of the

submicrometer-rough protrusions leaving submicrometer air pockets underneath, showing also locally a Cassie–Baxter-type wetting behaviour. For this case, we introduce in eq 6 a new local roughness factor f_{SLsub} that replaces R_{fsub}. f_{SLsub} is defined as the solid fraction of the rough pillar-top in contact with the liquid, taking values smaller than 1. The term f_{SLsub} when multiplied by f_{SL} will give the real fraction of the solid surface being in contact with the droplet. In other words, the eq 6 for a complete Cassie–Baxter state both in micrometer and submicrometer scale becomes

$$\cos\theta_a - \cos\theta_r = f_{SL\,sub} f_{SL} (\cos\theta_{a0} - \cos\theta_{ir0}) + H_r \quad (11)$$

Therefore, the general form of the modified equation for predicting the CAH for a superhydrophobic micropillar-patterned surface, with overall and local (on the top of the pillars) Cassie–Baxter type wetting behaviour would be:

$$\cos\theta_\alpha - \cos\theta_r = A_{CB} f_{SL} \quad (12)$$

$$A_{CB} = f_{SL\,sub} (\cos\theta_{\alpha 0} - \cos\theta_{r0}) + c \quad (13)$$

As a result, depending on the wetting state that the sprayed particles used in our experiments induce in the submicrometer scale, the CAH can be predicted by the following general equation:

$$\cos\theta_\alpha - \cos\theta_r = A f_{SL} \quad (14)$$

where A will be given from the eq 10 or 13, depending on the wetting state of the submicrometer scale. Considering also the eq 2, we obtain

$$\cos\theta_\alpha - \cos\theta_r = A[a^2/(a + d_{int})^2] \quad (15)$$

The parameters R_{fsub} and c or f_{SLsub} and c, can be related to each other after calculating the value of the parameter A from the theoretical curves obtained from the eq 15.

Figure 3 demonstrates the dependence of the experimental values of the advancing and receding angles on the d_{int} for the different patterns and coatings used in this work. Using eq 15 to fit these curves, we obtain the values of constant A for the PTFE and for the PTFE/NPs coated patterns. In particular, A equals to 2.9527 for the SU-8/PTFE/NPs substrates and 0.01529 for the SU-8/PTFE. Using these values, the wetting

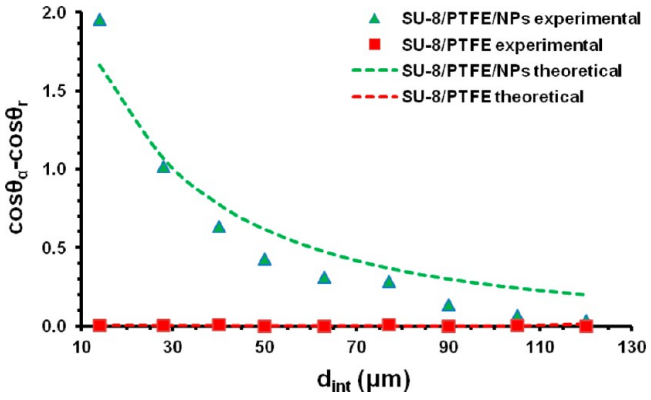

Figure 3. Experimental and theoretical curves of the CAH. The equation used to extract the theoretical curve is the 15: $\cos\theta_\alpha - \cos\theta_r = A[a^2/(a + d_{int})^2]$, where θ_α and θ_r are the advancing and receding contact angles, a is the square side of the pillar's top, d_{int} is the inter-pillar distance and the parameter A can be given by the eq 10 when $A = A_w$ or from the eq 13 if $A = A_{CB}$.

state of each system can be defined as discussed above by estimating the R_{fsub} or the f_{SLsub} as a function of the constant c by using the eqs 10 and 13. $\cos\theta_{\alpha 0} - \cos\theta_{r0}$ is measured experimentally by the advancing and receding contact angles on a flat PTFE surface (value = 0.46) and on a flat iron oxide surface where a thin layer of oleic acid is deposited (value = 0.78). Furthermore, as already discussed, for the Wenzel-type local wetting the roughness factor $R_{fsub} > 1$ should be considered whereas for the Cassie–Baxter-type local wetting, where air-pockets in the submicrometer scale exist, a solid-liquid fraction $0 < f_{SLsub} < 1$ has to be considered.

Similarly, the values of the parameter c are also restricted. According to Bhushan et al,[42] the CAH value in 6 is divided in two terms that depend on the work of adhesion and the pinning at the edges of the pillars. Both terms can have values from 0 to 2, underlying that their sum should be less than 2, since $0 < \cos\theta_\alpha - \cos\theta_r < 2$. Consequently, since $0 < S_f^2 < 1$ (eq 8), we can extract that $0 < c < 2$ (eq 7).

By introducing all the parameters found so far to the eqs 10 and 13, we can obtain the values of the R_{fsub} or f_{SLsub} for given values of c as shown in the Figure 4. In this figure it is depicted

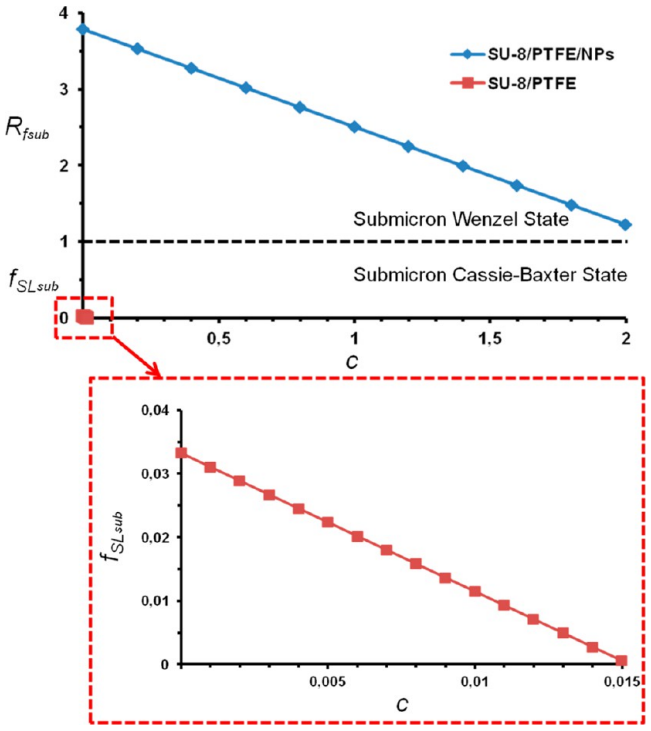

Figure 4. Dependence of the roughness factor and the solid–liquid fraction from the constant c for the SU-8/PTFE/NPs and the SU-8/PTFE samples, respectively.

with the dotted line in the graph the region where a submicrometer Cassie–Baxter state (characterized by a solid-liquid fraction f_{SLsub}) is separated by the submicrometer Wenzel state (characterized by a roughness factor R_{fsub}). Considering the restriction in the values that R_{fsub} and f_{SLsub} can obtain, we can conclude by their resulting values in which wetting state is our system. In the case of the SU-8/PTFE/NPs samples, the eq 10 is valid since the values obtained correspond to the presence of a roughness factor R_{fsub} ranging from 1.22 to 3.79 for $0 < c < 2$. On the contrary, in the case of the self-cleaning SU-8/PTFE samples, the values of the f_{SLsub} ($6 \times 10^{-4} < f_{SLsub} < 0.033$) are obtained from the eq 13 for $0 < c < 0.015$. For $c > 0.015$

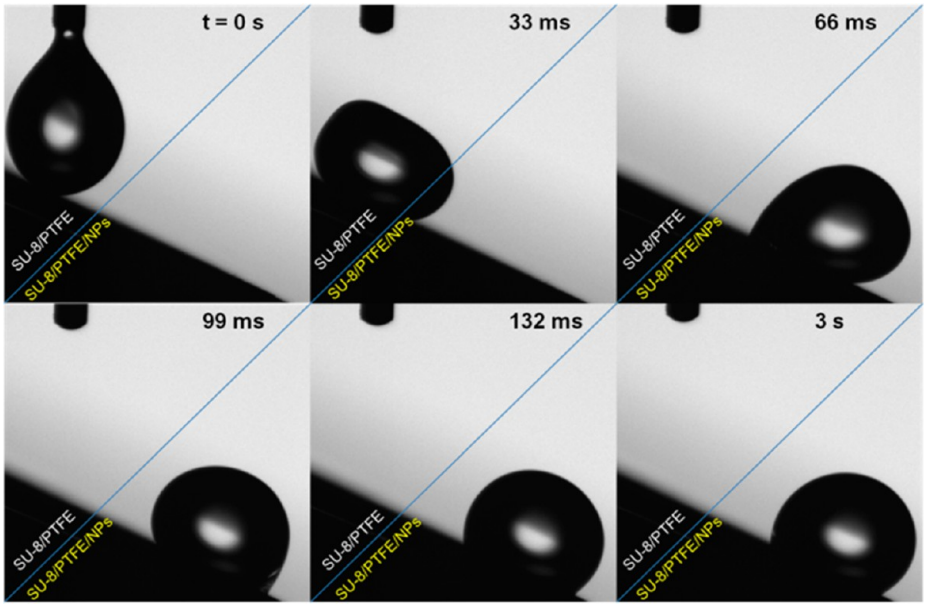

Figure 5. Frames of the movement of a water drop (10 μL) on an inclined surface (tilt angle 26°). The top left part of each image corresponds to SU-8/PTFE and the right bottom part to SU-8/PTFE/NPs. The frames are recorded every 33 ms except the last frame that is taken 3 s after the beginning of the drop movement and represents the new equilibrium state of the system.

negative f_{SLsub} values are obtained, that do not have any physical meaning. Thus, it is proved that in the SU-8/PTFE/NPs samples, Wenzel-type pinning effects in the submicrometer and nano-scale are dominant, which increase the CAH, while in the case of the SU-8/PTFE samples, the Cassie−Baxter state dominates also in the submicrometer-scale roughness.

Consequently, by modifying the pillar-spacing, the CAH can be controlled without altering the superhydrophobic characteristics of the surface. A similar mechanism has been described previously,[43] demonstrating that water adhesion can be increased by introducing nanofeatures on superhydrophobic paper fibers by plasma etching. Another group has also similarly claimed that the induced nanoroughness on a submicrometer-rough superhydrophobic surface contributes exclusively in the increase of the CAH.[16] However, both studies correlate the tuning of the water adhesion behaviour to the etching or spray parameters during the fabrication process without making a detailed discussion on the influence of the geometrical features on the water adhesion, but rather remain in qualitative statements. Furthermore, in accordance with our observations, Paxson et al.[41] showed that adding roughness scales does not necessarily decrease the water adhesion as one might have expected, but on the contrary a significant increase is possible to be observed. However, the common case where a multiple scale rough surface can be composed by hydrophobic materials with different chemistry that can promote Cassie or Wenzel transitions is neglected, in contrary to the present study.

Taking advantage the ability to spatially control the water adhesion we fabricated patterns ideal for applications regarding manipulation of water droplets, in terms of unforced movement, selective deposition and evaporation. As an example Figure 5 shows an inclined (tilt angle 26°) SU-8 micropatterned surface with d_{int} 28 μm, sprayed throughout with PTFE particles and subsequently with NPs only over a selected area masking the rest with a glass slide. The part of the surface covered with PTFE particles shows very low adhesion whereas the part covered with NPs is highly water adhesive. Therefore, when a water droplet is placed on the self-cleaning area it starts rolling, until it comes in contact with the highly adhesive zone, where it is immobilized.

Figure 6 presents SU-8 pillars covered with a PTFE layer, on the top of which a NPs layer is spayed locally through an aperture. In this way a NPs-coated area with perimeter 2.67 mm onto the SU-8/PTFE pillared sample is obtained. The spot covered with NPs is superhydrophobic like the rest of the surface but in contrast, it has higher water adhesion. In the sequence of Figure 6a−f is shown a drop initially in contact with the self-cleaning part of the surface, where it easily slides dragged by a syringe from which it was dispensed, without

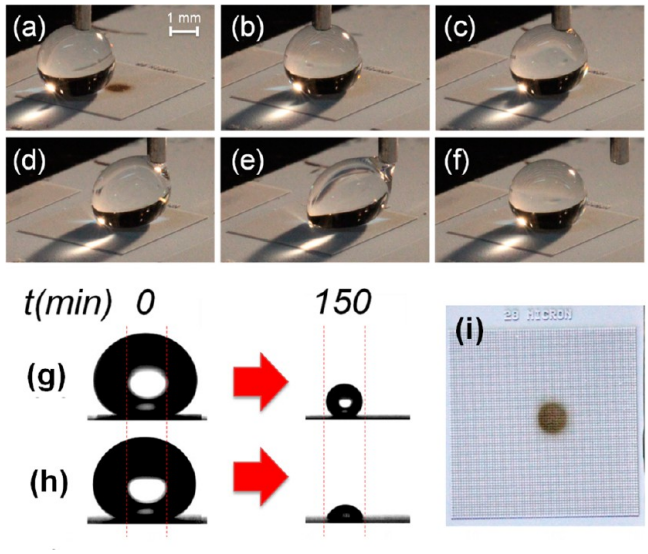

Figure 6. (a−f) Image sequence of the drop moving with constant speed across the SU-8/PTFE micro-pattern. The dark brown area in panel a is an SU-8/PTFE/NPs disk. Each frame (a−f) corresponds to a 600 μm step. (g) SU-8/PTFE pattern and (h) on a circular disk of SU-8/PTFE/NPs as shown in panel i on the SU-8/PTFE pattern. The dotted red lines mark the diameter of the disk.

dx.doi.org/10.1021/am404565a | ACS Appl. Mater. Interfaces 2014, 6, 1036−1043

being released (Figure 6a,b). However, when the drop comes in contact with the sticky area covered by the NPs (frames b, c, d, e) it adheres on it and it is eventually detached from the syringe (frame f). In this way, drops can be entrapped onto purposely designed areas (see Video in the Supporting Information). Using this technique of spontaneous deposition of almost spherical water droplets to purposely designed areas of the substrate, we envision applications like targeted delivery of biomolecules or drugs for local chemical reactions. The water droplets can incorporate such molecules which will be selectively deposited after their evaporation. In fact, in Figure 6g is demonstrated that the APCA of a large drop (25 μL) deposited on a SU-8/PTFE pillared sample remains during evaporation always to the superhydrophobic regime, even when the drop becomes very small prior to complete evaporation, due to the very low adhesion. An identical drop placed centralized onto the SU-8/PTFE/NPs spot presented in Figure 6i, experiences both the SU-8/PTFE (self-cleaning) and the SU-8/PTFE/NPs ("sticky" = superhydrophobic) surface, since it is big enough to include the entire SU-8/PTFE/NPs disk into its perimeter. Before the complete drop evaporation, (at 150 min (Figure 6h)), the contact line is equal to the perimeter of the area sprayed with NPs (2.67 mm) and significantly larger than the one obtained on the SU-8/PTFE surface after the same time (Figure 6g). Therefore the area of deposition of water-soluble substances can be very well controlled with the proposed technique.

4. CONCLUSIONS

We present a simple method for the realization of surfaces with controlled wetting behaviour. Surfaces with triple-scale hierarchical roughness are obtained by the spray-coating with PTFE sub-micrometer particles and hydrophobically capped iron oxide NPs onto SU-8 micro-pillars. The PTFE layer makes the pillars superhydrophobic with extremely low CAH. The successive coating of NPs tunes the surfaces' CAH from extremely high to quite low as the inter-pillar distance increases, while the superhydrophobicity is preserved. The experimental results are evaluated and confirmed by developing a theoretical model for the prediction of CAH on multi-scale rough hierarchical surfaces. The controlled water adhesion characteristics of the patterns can be "erased" and "rewritten" by applying successive coating layers of the appropriate particles. In this way, the substrates can be used multiple times to perform different functions. Following the proposed spraying strategy it is possible to form self-cleaning surfaces with localized highly adhesive areas that can be used for the localized deposition and controlled evaporation of liquid drops. The fabricated patterns can be excellent candidates for the development of microfluidic devices, smart surfaces, biotechnological, and novel antifouling materials.

■ ASSOCIATED CONTENT

Supporting Information

Video demonstrating the localized deposition of a water droplet on a superhydrophobic, surface energy trap. This information is available free of charge via the Internet at http://pubs.acs.org/.

■ AUTHOR INFORMATION

Corresponding Authors

*E-mail: am2vy@virginia.edu.
*E-mail: athanassia.athanassiou@iit.it.

Present Address

[⊥]Athanasios Milionis: Department of Mechanical & Aerospace Engineering, University of Virginia, 122 Engineer's Way, 22904 Charlottesville, VA, United States

Author Contributions

The manuscript was written through contributions of all authors. All authors have given approval to the final version of the manuscript.

Notes

The authors declare no competing financial interest.

■ ACKNOWLEDGMENTS

The authors thank Mr. Paolo Cazzato, Mr. Diego Mangiulo, and Mr. Gianmichele Epifani, National Nanotechnology Laboratory (NNL), CNR Istituto Nanoscienze, c/o Distretto Tecnologico, Lecce, Italy as well as Dr. Leonardo Sileo and Mr. Francesco Guido, Center for Biomolecular Nanotechnologies, Istituto Italiano di Tecnologia@UNILE for their contribution.

■ ABBREVIATIONS

APCA = apparent contact angle
CAH = contact angle hysteresis
PTFE = polytetrafluoroethylene
NP = nanoparticle
d_{int} = interpillar distance
SEM = scanning electron microscopy

■ REFERENCES

(1) Quere, D. *Rep. Prog. Phys.* **2005**, *68*, 2495−2532.
(2) Tourkine, P.; Le Merrer, M.; Quere, D. *Langmuir* **2009**, *25*, 7214−7216.
(3) Milionis, A.; Giannuzzi, R.; Bayer, I. S.; Papadopoulou, E. L.; Ruffilli, R.; Manca, M.; Athanassiou, A. *ACS Appl. Mater. Interfaces* **2013**, *5*, 7139−7145.
(4) Chapman, J.; Regan, F. *Adv. Eng. Mater* **2012**, *14*, B175−B184.
(5) Tsougeni, K.; Papageorgiou, D.; Tserepi, A.; Gogolides, E. *Lab Chip* **2010**, *10*, 462−469.
(6) Hong, L.; Pan, T. *J. Microelectromech. Syst.* **2010**, *19*, 246−253.
(7) Weng, C. J.; Chang, C. H.; Peng, C. W.; Chen, S. W.; Yeh, J. M.; Hsu, C. L.; Wei, Y. *Chem. Mater.* **2011**, *23*, 2075−2083.
(8) Webb, H. K.; Hasan, J.; Truong, V. K.; Crawford, R. J.; Ivanova, E. P. *Curr. Med. Chem.* **2011**, *18*, 3367−3375.
(9) Oner, D.; McCarthy, T. J. *Langmuir* **2000**, *16*, 7777−7782.
(10) Quere, D.; Lafuma, A.; Bico, J. *Nanotechnology* **2003**, *14*, 1109−1112.
(11) Feng, L.; Zhang, Y.; Xi, J.; Zhu, Y.; Wang, N.; Xia, F.; Jiang, L. *Langmuir* **2008**, *24*, 4114−4119.
(12) Lai, Y. K.; Chen, Z.; Lin, C. J. J. *Nanoeng. Nanomanuf.* **2011**, *1*, 18−34.
(13) Villafiorita Monteleone, F.; Caputo, G.; Canale, C.; Cozzoli, P. D.; Cingolani, R.; Fragouli, D.; Athanassiou, A. *Langmuir* **2010**, *26*, 18557−18563.
(14) Wu, D.; Wu, S. Z.; Chen, Q. D.; Zhang, Y. L.; Yao, J.; Yao, X.; Niu, L. G.; Wang, J. N.; Jiang, L.; Sun, H. B. *Adv. Mater.* **2011**, *23*, 545−549.
(15) Verho, T.; Korhonen, J. T.; Sainiemi, L.; Jokinen, V.; Bower, C.; Franze, K.; Franssila, S.; Andrew, P.; Ikkala, O.; Ras, R. H. A. *Proc. Natl. Acad. Sci. U.S.A.* **2012**, *109*, 10210−10213.
(16) Teisala, H.; Tuominen, M.; Aromaa, M.; Stepien, M.; Makela, J. M.; Saarinen, J. J.; Toivakka, M.; Kuusipalo, J. *Langmuir* **2012**, *28*, 3138−3145.
(17) Zhao, X. D.; Fan, H. M.; Liu, X. Y.; Pan, H.; Xu, H. Y. *Langmuir* **2011**, *27*, 3224−3228.
(18) Zhu, S.; Li, Y.; Zhang, J.; Lu, C.; Dai, X.; Jia, F.; Gao, H.; Yang, B. *J. Colloid Interface Sci.* **2010**, *344*, 541−546.

(19) Li, J.; Liu, X.; Ye, Y.; Zhou, H.; Chen, J. *J. Phys. Chem. C* **2011**, *115*, 4726−4729.
(20) Liu, X.; Ye, Q.; Yu, B.; Liang, Y.; Liu, W.; Zhou, F. *Langmuir* **2010**, *26*, 12377−12382.
(21) Ishii, D.; Yabu, H.; Shinomura, M. *Chem. Mater.* **2009**, *9*, 1799−1801.
(22) Cheng, Z.; Lai, H.; Du, M.; Zhu, S.; Zhang, N.; Sun, K. *Soft Matter* **2012**, *8*, 9635−9641.
(23) Balu, B.; Berry, A. D.; Hess, D. W.; Breedveld, V. *Lab Chip* **2009**, *9*, 3066−3075.
(24) Milionis, A.; Martiradonna, L.; Anyfantis, G. C.; Bayer, I. S.; Fragouli, D.; Athanassiou, A. *Colloid Polym. Sci.* **2013**, *291*, 401−407.
(25) Elbert, B.; Bhushan, B. *J. Colloid Interface Sci.* **2012**, *384*, 182−188.
(26) Li, X.; Shen, J. *Chem. Commun.* **2013**, *49*, 10016−10018.
(27) Bormashenko, E.; Stein, T.; Pogreb, R.; Aurbach, D. *J. Phys. Chem. C* **2009**, *113*, 5568−5572.
(28) Zhao, N.; Xie, Q.; Kuang, X.; Wang, S.; Li, Y.; Lu, X.; Tan, S.; Shen, J.; Zhang, X.; Zhang, Y.; Xu, J.; Han, C. C. *Adv. Funct. Mater.* **2007**, *17*, 2739−2745.
(29) Cho, W. K.; Choi, I. S. *Adv. Funct. Mater.* **2008**, *18*, 1089−1096.
(30) De Angelis, F.; Gentile, F.; Mecarini, F.; Das, G.; Moretti, M.; Candeloro, P.; Coluccio, M. L.; Cojoc, G.; Accardo, A.; Liberale, C.; Zaccaria, R. P.; Perozziello, G.; Tirinato, L.; Toma, A.; Cuda, G.; Cingolani, R.; Di Fabrizio, E. *Nat. Photonics* **2011**, *5*, 682−687.
(31) Marmur, A. *Soft Matter* **2006**, *2*, 12−17.
(32) Cassie, A. B. D.; Baxter, S. *Trans. Faraday Soc.* **1944**, *40*, 546−551.
(33) Wenzel, R. N. *Ind. Eng. Chem.* **1936**, *28*, 988−994.
(34) Zhu, L.; Feng, Y.; Ye, X.; Zhou, Z. *Sens. Actuators, A* **2006**, *130*, 595−600.
(35) Caputo, G.; Cortese, B.; Nobile, C.; Salerno, M.; Cingolani, R.; Gigli, G.; Cozzoli, P. D.; Athanassiou, A. *Adv. Funct. Mater.* **2009**, *19*, 1149−1157.
(36) Lee, J. B.; Gwon, H. R.; Lee, S. H.; Cho, M. *Mater. Trans.* **2010**, *51*, 1709−1711.
(37) Yeh, K. Y.; Chen, L. J.; Chang, J. Y. *Langmuir* **2008**, *24*, 245−251.
(38) Xu, W.; Choi, C. H. *Phys. Rev. Lett.* **2012**, *109*, 024504.
(39) Lv, C.; Yang, C.; Hao, P.; He, F.; Zheng, Q. *Langmuir* **2010**, *26*, 8704−8708.
(40) Reyssat, M.; Quere, D. *J. Phys. Chem. B* **2009**, *113*, 3906−3909.
(41) Paxson, T.; Varanasi, K. K. *Nat. Commun.* **2013**, *4*, 1492.
(42) Bhushan, B.; Nosonovsky, M.; Jung, Y. C. *J. R. Soc. Interface* **2007**, *4*, 643−648.
(43) Balu, B.; Kim, J. S.; Breedveld, V.; Hess, D. W. *J. Adhes. Sci. Technol.* **2009**, *23*, 361−380.